Research Square

Preprints are preliminary reports that have not undergone peer review.
They should not be considered conclusive, used to inform clinical practice,
or referenced by the media as validated information.

Mg alloy surface immobilised with caerin peptides acquires enhanced antibacterial ability and improved corrosion resistance

Tianfang Wang
University of the Sunshine Coast https://orcid.org/0000-0002-4876-7767
Guoying Ni
University of the Sunshine Coast
Tsuyoshi Furushima
The University of Tokyo
Hui Diao
University of Queensland
Pingping Zhang
First People's Hospital of Foshan
Shu Chen
First People's Hospital of Foshan
Conor E. Fogarty
University of the Sunshine Coast
Zhengyi Jiang
University of Wollongong
Xiaosong Liu (xiaosongl@yahoo.com)
University of the Sunshine Coast
Hejie Li (hejiel2003@gmail.com)
University of the Sunshine Coast

Research Article

Keywords: Antibacterial activity, caerin peptide, in vitro corrosion resistance, Mg alloy, chemical click reaction, peptide immobilisation

Posted Date: October 14th, 2020

DOI: https://doi.org/10.21203/rs.3.rs-92270/v1

License: This work is licensed under a Creative Commons Attribution 4.0 International License.
Read Full License

Version of Record: A version of this preprint was published at Materials Science and Engineering: C on October 14th, 2020. See the published version at https://doi.org/10.1016/j.msec.2020.111819.

Mg alloy surface immobilised with caerin peptides acquires enhanced antibacterial ability and improved corrosion resistance

Tianfang Wang[1], Guoying Ni[1, 2], Tsuyoshi Furushima[3], Hui Diao[4], Pingping Zhang[5], Shu Chen[5], Conor E. Fogarty[1], Zhengyi Jiang[6], Xiaosong Liu[1,5*], Hejie Li[1, 3*]

1. Genecology Research Centre, University of the Sunshine Coast, Maroochydore DC, QLD 4558, Australia.

2. The First Affiliated Hospital/School of Clinical Medicine of Guangdong Pharmaceutical University, Guangzhou 510080, China

3. Institute of Industrial Science, Department of Mechanical and Biofunctional Systems, the University of Tokyo, 4-6-1, Komaba, Meguro, Tokyo 153-8505, Japan.

4. Centre for Microscopy and Microanalysis, University of Queensland, St. Lucia QLD 4072, Australia

5. Cancer Research Institute, First People's Hospital of Foshan, Foshan, Guangdong 528000, China

6. School of Mechanical, Materials, Mechatronic and Biomedical Engineering, Faculty of Engineering and Information Sciences, University of Wollongong, Northfields Ave, Wollongong NSW 2522, Australia.

Running title: Caerin coating Mg alloy shows higher corrosion resistant and bactericidal ability

Authorship:

Tianfang Wang and Guoying Ni are equally co-first authors, contributed equally to this study.

***Correspondence:**

Hejie Li, PhD, Email: hejiel2003@gmail.com

Xiaosong Liu, PhD&MD, Email: xiaosongl@yahoo.com

Abstract

Magnesium (Mg) has mechanical properties similar to human bones and Mg alloy is considered ideal medical implant material. However, the high velocity of degradation inside the human inner environment severely hampers the usage of Mg alloys. In this study, caerin peptide 1.9 (F3) and a modified sequence of caerin 1.1 (F1) with anti-bacterial activity, were covalently immobilised on the surface of Mg alloys by plasma chemical click reaction. The *in vitro* antibacterial activity and corrosion resistance of these caerin peptide-immobilised Mg alloys were investigated in Dulbecco's Modified Eagle Medium (DMEM) solution. Un-immobilised Mg alloy sample, blank drug-sensitive tablet (BASD) and a commonly used antibiotics Tazocin were used for comparison. Results showed that peptide immobilised Mg samples showed significant improved corrosion resistance and prolonged antibacterial effect compared to non-immobilised Mg alloy and free caerin peptides. Furthermore, annealing or extruding treatment of Mg alloys improved the behaviours of corrosion resistance and antibacterial property. These results indicate that coating Mg alloy with caerin peptides improves the corrosion resistance *in vitro* and increases the alloy's antibacterial ability. The mechanism underlying the prolonged antibacterial effect for annealed Mg alloys immobilised with the peptides (especially F3) remains unclear, which worth further experimental and theoretical investigation.

Key words: Antibacterial activity; caerin peptide; *in vitro* corrosion resistance; Mg alloy; chemical click reaction; peptide immobilisation

1. Introduction

Fractures cause a considerable public health burden worldwide and are usually caused by accidents and/or related to osteoporosis. It is estimated that 1 in 2 women over 50 years of age will suffer one fracture, as will 1 in 5 men [1]. In United Kingdom, the overall annual fracture incidence is 3.6%, and age-standardised lifetime fracture prevalence is estimated to be 38.2% [2]. After trauma or surgical intervention, often it is essential to fix bone fragments together to immobilise the fragments and permit healing. Traditional bone fixation materials, such as titanium alloy and stainless steel, remain widely used. However, they are significantly different from human bone tissues, with differences in elastic modules and mechanical strengths [3, 4]. These materials also result in stress shielding and local pH increases due to the release of metal ions or hydrogen [5], which may lead to inflammation and subsequent bone loss and failure of the metal implants [6]. Besides personal suffering, this produces substantial socio-economic losses. Therefore, fixation materials with better biological compatibility are urgently needed.

Magnesium (Mg) is the lightest metal (ranging from 1.74 to 2.0 g/cm^3), weighing 33% and 77% less than aluminium and steel, respectively [7]. Mg shows similarities to human bones with respect to strength and Young's moduli [8]. These characteristics greatly reduce the risk of stress shielding effects in the human body, making it an ideal candidate for human bone fracture internal fixation. In addition, Mg is a necessary component of the human metabolism, making it a more biocompatible than other fixation materials. Roughly 60% of Mg is stored in the bone as skeletal Mg, one third of which resides on cortical bone either on the surface of hydroxyapatite or in the hydration shell around the crystal [9, 10]. Most bone Mg is likely deposited as an integral component of the apatite crystal and be reabsorbed by bones when released. Intracellularly, Mg is vital to numerous physiological functions, including providing energy in the cells as fundamental component of ATP, involvement in the synthesis of lipid, protein, and nucleic acid as a cofactor of enzymes, and stabilising cell membranes. It also antagonises calcium [11] and functions as a signal transmitter [12].

Although pure Mg has recently been shown to have the property of anti-bacterial growth both *in vitro* and *in vivo* [13], it increases the pH value of the local humoral environment and potentially cause alkalosis, local inflammatory reactions and cell death [14]. In addition, its degradation rates are generally very high. These problems severely limit the commercial usage of Mg alloys for bone grafts or fixation materials [15-17]. Thus, many attempts have been made to improve the corrosion resistance of Mg, including various alloying [18-22], processing [23-27], and protective coating [28-32].

Another complication for internal implanting is periprosthetic infections (PPI). An implanted material surface may accumulate bacteria, leading to bacterial colonisation and the formation of bacteria biofilm [14, 33, and 34]. To manage PPI, treatments including antimicrobial treatment, implant removal and surgical revision may be conducted, however each of these increase the patient's physical stress and economic costs [35, 36]. Many studies have focused on the development of novel medical biomaterials with antibacterial activities, including metal implants with bacterial clearance properties.

Antimicrobial peptides (AMPs) are generally short and positively charged peptides, usually between 12 and 50 amino acids, and commonly referred to as host defence peptides (HDPs). AMPs have potent antibacterial, antiviral, and antifungal activity and are ubiquitous among multicellular eukaryotes, with most plant and animal species expressing dozens of distinct AMP genes in epithelial tissues and in response to infection [37]. Therefore, AMPs become a potential candidate for the PPI treatment of internal implant. With a controlled release of the AMP, a three-layer coating of a broad-spectrum AMP (HHC-36, KRWWKWWRR-OH) on TiO_2 nanotube was confirmed to be highly effective against both *Staphylococcus aureus* and *Pseudomonas aeruginosa* bacteria, without observable cytotoxicity to osteoblast-like cells (MG-63) [38]. A gentamicin-loaded mesoporous bioactive glass was developed for a controlled antibiotic delivery system to tackle orthopedic PPIs, which prevented biofilm formation by *S. aureus* and *S. epidermidis*, with better biocompatibility with human bone marrow stromal cells (HBMSCs) than non-mesoporous biological glass (NBG) [39]. Zn/Ag co-implanted titanium by plasma immersion ion implantation also showed excellent osteogenic activity and antibacterial ability and has potential applications in orthopedic and dental implants [40]. However, few studies have focused on improving the antibacterial effect of Mg and its alloys by employing AMPs.

As typical HDPs, peptides extracted from amphibians displayed the ability to kill bacteria by targeting the bacterial membrane [41, 42]. More than 200 HDPs have been identified from epidermal secretions of Australian frogs and toads [43]. Research has shown that Australian frog-derived caerin peptides were potent membrane-active peptides, which can inhibit the formation of nitric oxide [44]. Caerin peptides inhibit the growth of broad spectrum of bacteria [45-50], fungi [45], and some cancer cells [45, 51] both *in vitro* and *in vivo* [52, 53]. In the current study, we attempted to immobilise the surface of the Mg alloys with caerin peptides to develop biomimetic Mg alloys with improved corrosion resistance and antibacterial activity.

2. Materials and methods

2.1 Chemicals

Polyurethane (PU, grade MQ100, Selectophore™), chloroform (purity>99.5%), acrylic acid, N-hydroxysuccinimide, 1-ethyl-3-(3-dimethylaminopropyl) carbodiimide, sodium phosphate and phosphate buffered saline were purchased from Sigma Aldrich (St. Louis, MO, USA). Dulbecco's Modified Eagle Medium (DMEM) was purchased from Gibco (Carlsbad, CA, USA).

2.2 Mg alloy preparation

Two types of Mg alloy materials were used: i) cold extruded Mg AZ31 and ii) fully annealed Mg AZ31 under a no interference atmosphere (vacuum or inert gas). The two materials were manufactured into a thin plate with a dimeter of 4.4 mm and thickness of 2 mm (**Fig. 1A**). The samples were grinded by 400 grit silicon carbide paper for 1-3 min to remove the original oxide layer and polished by 800-2400 grit silicon carbide paper for 2-5 min to improve the sample surface qualities and obtain homogeneous roughness. All the samples were rotated 90° to ensure that the next step of grinding and polishing removed the scratches generated prior. Before experimentation, all samples were ultrasonically cleaned in 70% ethanol for 5 mins to remove any surface residues. All the samples were ultrasonically rinsed in distilled water for 3 mins. Cleaned alloys were placed under UV radiation for 30 mins on each side for sterilisation [54]. Sterilised AZ31 samples were used as non-immobilised controls. To stabilise the surface prior to coating, a group of AZ31 samples were subjected to a fully annealed heat treatment to eliminate the original textures and microstructures. They were heated to 330-350 ℃ in an inert gas atmosphere (Argon), kept for 3-5 hrs, and cooled in furnace.

Fig. 1. Mg alloy fabrication and peptide immobilisation procedure. (A) Schematic of Mg samples and all size parameters; (B) Surface modification of polyurethane coating Mg alloy by chemical click-reaction using O_2 plasma; (C) Mg alloy immobilised by polyurethane and immobilisation of F1 or F3 on surface.

2.3 Peptide synthesis

The sequence modified caerin 1.1 (F1) (GLLSVLGSVAKHVLPHVLPHVVPVIAEHL-NH_2), caerin 1.9 (F3) (GLFGVLGSIAKHVLPHVVPVIAEKL-NH_2) and the control peptide P3 (GTELPSPPSVWFEAEF-OH) were synthesised by ChinaPeptides Co., LTD (Shanghai, China). The purity of the peptides was >99% as determined by ChinaPeptides Co., LTD using reverse-phase HPLC.

2.4 Chemical click reaction and peptide immobilisation

Since peptides cannot covalently bond with metal directly, polyurethane was layered over the surface using a chemical click reaction. Briefly, polyurethane was thoroughly dissolved in chloroform solution at a ratio of 3% (W/V). The two ultrasonic cleaned Mg-based alloys AZ31 samples were immersed into polyurethane/chloroform solution for 60 min with intermittently stirring. The two Mg-alloy materials uniformly immobilised with polyurethane were taken out of the solution and dried in a watch glass for 16 hrs to form a uniform, tight and stable polyurethane coating layer on the metal surface. The immobilised metal samples were treated in a plasma reactor (MiniFlecto®, Plasma Technology GmbH, Herrenberg, Germany) with oxygen plasma at 2.45 GHz for 1 min and placed in the atmospheric environment for 15 min to promote the formation of surface peroxy groups and hydroxyl groups. The metal was transferred back to the plasma reactor, the vacuum was adjusted to 26.7 and slowly passed in the acrylic vapor to 66.7 Pa. The metal was taken out after one min of reaction, washed with an ultrasonic cleaner for 10 min, transferred to a mixed aqueous solution (pH 5.0) of 1.25 mg/ml N-hydroxysuccinimide and 5 mg/ml 1-ethyl-3-(3-dimethylaminopropyl) carbodiimide and shaken and stirred at 4°C for 20 hrs. The process of chemical click-reaction is shown in **Fig. 1B**.

The synthesised F1 and F3 were dissolved in a 0.1 M sodium phosphate solution to prepare a 5 mM homogeneous solution. The surface-activated polyurethane-coated Mg alloy sample was immersed in peptide solution at 4 °C for 20 hrs and ultrasonically washed twice in ultrapure water for 10 min. The preparation was completed by drying F1/F3 immobilised Mg alloys under a fume hood, which were subjected to the following bioassay (**Fig. 1C**).

2.5 Coverage of peptides

Normally, the amount of immobilised peptide can be calculated by the equilibrium adsorption capacity [55]. In this study, peptides might be adsorbed on the PU surface via weak interaction, e.g., Van der

Waals attraction. However, we expected the amount of peptides adsorbed on the PU surface would be relatively low, since the samples were ultrasonically washed twice in ultrapure water for 10 min post peptide immobilisation (see **Section 2.4**), which should significantly remove those peptides physically adsorbed on the PU surface. Thus, we did not measure the physical adsorption capacity, but used the coverage of peptides to evaluate the amount of the immobilised peptides.

Post the peptide immobilisation step, we measured the concentration of peptides left in the solution for immobilisation and MilliQ water used to ultrasonically wash the samples. We considered the difference in total peptide corresponding to the amount of peptide linked to the coating layer. The concentration of peptides in the MilliQ water used for the second wash cannot be detected using the current BCA assay (Pierce™ BCA Protein Assay Kit, Catalogue number: 23227, Thermoscientific), thus only the peptides in the water for the first wash was included. Thus, we have added the following equation to estimate the coverage of different peptides. The calculation showed that F3 had higher coverage values for 1E and AZ31, while the coverage on AP was similar with respect to F1 or F3.

$$m_c = m_t - m_l - m_w \tag{1}$$

where, m_c is the mass of peptide covalently bonded to the coating layer (mg), m_t is the mass of total peptide used in peptide immobilisation step (mg), m_l and m_w represent the masses of peptide left in the tubes for peptide immobilisation and ultrasonic wash (mg), respectively.

$$C = \frac{m_c/MM}{S} \tag{2}$$

where, C is the coverage of the peptide (nmol/mm^2), MM is the molar mass of the peptide used in immobilization (molar mass of peptide F1 is 3030.68 g/mol and molar of peptide F3 is 2593.19 g/mol) and S is the surface area of the Mg alloy specimen (mm^2).

2.6 Bonding force test

Bonding force between the PU coating and the substrate mainly depends on the surface morphology (surface roughness and surface asperity) and bonding area. It can be tested qualitatively by following methods: X-cut tape test, Cross-cut test and Pull off test for adhesion. In this study, the Cross-cut test was employed with certain scale according to the international standard [56, 57] and related literature [58]. All the sample's surfaces before and after the test were mapped by Leica DFC 550 Fluorescence/Light Microscope.

2.7 *In vitro* corrosion test

Corrosion samples (the original two Mg alloys AZ31 in different treatment states and two Mg alloys immobilised with peptides F1 and F3 respectively) are uniformly made into small-sized Mg pieces with a diameter of 4.4 mm and a thickness of 2 mm. The dimensional tolerance is 0.002 mm. Surface cleaning of the original two Mg alloys AZ31 with two different treatment states and two Mg alloy samples that respectively form F1 and F3 polypeptide coatings through cleaning with pure water and in an ultrasonic cleaner for 3-5 min to remove surface residues and adhesives. All the peptide-immobilised AZ31 samples were immersed in DMEM and kept in a 37°C thermostat incubator for 120 hrs. DMEM was selected to simulate the physiological condition. During the *in vitro* corrosion process the two parameters were used to assess the corrosion resistance of the peptide-immobilised AZ31 samples, including the weight variation of the sample and pH value of the DMEM medium.

2.7.1 pH value

During the *in vitro* corrosion test, the pH value of corrosion solution (DMEM culture media) was tested at 0, 0.5, 1, 2, 4, 8, 16, 32 etc. hrs by the Cyberscan pH510 Bench Meter. Prior to pH value testing the meter was calibrated and after the test the detector was cleaned by pure water. The corrosion of Mg alloys usually take place as follows: Mg alloy reacts with water to produce like ionic magnesium Mg and the hydroxide in the solution increases, causing the pH value to rise as shown in **Eqns. (3) and (4)**.

$$Mg + 2H_2O = Mg^{2+} + 2OH^- + H_2 \quad (3)$$

$$pH_{[solution]} = -\lg [H^+] = 14 - (-\lg [OH^-]) \quad (4)$$

2.7.2 Weight change

At designated time points along the incubation, the samples were taken out from their tubes, washed with deionised water and dried in a biosafety fume hood at room temperature. Then, they were weighed by an electronic balance (Shimadzu electronic balance AUW220D) and returned to the respective tubes. Variations in sample weight were recorded and analysed accordingly.

2.8 Surface characterisation

After the 120-hr *in vitro* corrosion test, all samples were washed in phosphate buffer saline (PBS buffer solution) for 3-5 min and dried in a biosafety fume hood at the room temperature. Due to poor conductivity of the peptide-immobilised two group samples, all samples were carbon-sprayed by Q150T turbomolecular pumped coater before observation. After carbon spray, all samples including peptide-immobilised and no peptide-immobilised samples, were fixed to the sample stages with double-layer conductive tapes. FEI SCIOS SEM/FIB Dual Beam system was employed to scan all peptide-immobilised samples and no peptide-immobilised samples to assess morphology, distribution and microstructure.

The elemental composition of caerin peptide-coating was analysed using energy dispersive X-ray spectroscopy (EDS) coupled with scanning electron microscope JEOL 6010 SEM. Carbon is the most important component of peptides and Mg oxide is the main product during in vitro corrosion test. By analysing the carbon component and Mg oxide we can understand the peptide evolution on the samples' surface and the quantity of Mg corroded during the test. Therefore, the EDS analysis primarily focussed on the variation of these two components.

2.9 Bacteriostatic test

After the surface cleaning of the original two Mg alloys AZ31 with two different treatments the two Mg alloy samples were immobilised by F1 and F3 polypeptides through being cleaned by distilled water in an ultrasonic cleaner for 3-5 min to remove impurities and adhesives from the surface. The cleaned samples were put into a bacteriostatic petri dish to conduct a 100-hr bacteriostatic test on drug-resistant *S. aureus* in a 37°C temperature incubator. The methicillin-resistant *S. aureus* (MRSA, GDM1.1263) were cultured to a logarithmic phase and adjust the suspension concentration of MH (Mueller-Hinton) medium to 2.0×10^5 CFU/ml. A sterile cotton swab was used to dip the bacteria solution and squeeze the tube wall several times to remove the excess. The swab was used to smear the entire M-H drug-sensitive agar plate (Guangzhou Yuanming Bio Company). Aliquots of 30 μg of F1 and F3 peptides were added drug-sensitive papers (OXOID, UK) and the papers were pasted on M-H agar plates. The plates were inverted and incubated at 37°C overnight. A volume of 30 μg piperacillin sodium and tazobactam sodium with a weight ratio of 8:1 (Tazocin, Haikou Qili Pharmaceutical Co., Ltd,

Haikou) and blank drug-sensitive tablets (BASD, Thermo Fisher Scientific, Shanghai) and two original AZ31 Mg alloys were used as controls. A Vernier calliper was used to measure the size of the zone of inhibition.

3. Results

3.1 Coverage of peptides

This study was to develop an approach to chemically immobilise caerin peptides onto PU coating magnesium alloy. Thus, as shown in **Fig. 1B**, there should be a single layer of peptides immobilised on the surface via covalent bonding, which could enable multiple contacts with bacteria, potentially contributing to the prolonged antibacterial effect. Thickness of the polyurethane on the magnesium alloy surface was measured. Average thickness of polyurethane coating is about 135 μm.

The results of coverage of peptides have been added with the data recorded in **Table S1**. For peptide F3, extruded AZ31 has the highest coverage, which is about 5.65 nmol/mm2, followed by annealed AZ31 with a peptide coverage of 5.57nmol/mm2. Pure Mg has the lowest coverage for peptide F3, which is 5.49 nmol/mm2. For peptide F1, the coverage order is as: pure Mg (5.49 nmol/mm2), annealed AZ31 (5.47 nmol/mm2) and extruded AZ31 (5.14 nmol/mm2). Overall, annealed AZ31 has the better coverage for caerin peptides F1 and F3.

3.2 Bonding force test

Bonding force test results are shown in **Fig. 2**. Original surface of Mg specimen is shown in **Fig. 2A**. **Fig. 2B** shows the surface of PU coated Mg alloy. As shown in **Fig. 2 C**, after the test, 5 % -10 % small flakes of the coating were detached at intersections, which fell in a reasonably rate of bonding force [57].

Fig. 2. Surfaces of different specimens: (A) Mg alloy only; (B) Mg alloy with PU coating, and (C) PU coated Mg alloy after bonding force test

3.3 *In vitro* corrosion test

The microstructure of two types of Mg alloys used in coating were compared (**Figs. 3A** and **3B**). Annealed AZ31 has equiaxed grain with average grain size of 15.85 μm, there are few annealed twins distributed inside grain or trans-grains (**Fig. 3A**). While cold extruded AZ31 has typcial cold deformed microstructure with average grain size of 9.57 μm and many cold-extruded twining texture which distributed along the related deformation axis, and inside or trans-grains (**Fig. 3B**).

Fig. 3. Microstructure of annealed AZ31 (A) and cold extrude AZ31 (B). Analysis of pH of different samples during *in vitro* corrosion test: (C) Extruded AZ31, extruded AZ31 immobilised by F1, and extruded AZ31 immobilised by F3. (D) Annealed AZ31, annealed AZ31 immobilised by F1, and annealed AZ31 immobilised by F3.

The corrosion of Mg produces Mg^{2+}, reduces H_2O and releases H_2 gas and hydroxyl ions $[OH]^-$ into the medium environment. The weight change of the Mg materials with and without peptide immobilisation were recorded at selected time points along the incubation time of 120 hrs. The results of the *in vitro* corrosion test were shown in **Table S2**. Results showed that compared to the non-immobilised sample, peptide-immobilised sample showed improved corrosion resistance and excellent antibacterial ability. It is probable that the different corrosion resistance and antibacterial ability are a result of different peptides.

The methods used in the current study, including the changes of weight and pH value before and after immersion test, are direct and effective approaches to check the outcomes of corrosion reaction. Indeed, electrochemical techniques is also an important approach to study anticorrosion performance, which will be an ideal approach in the future study for corrosion resistance of coating of PU immbolised caerin petides on Mg alloys.

3.3.1 pH value

As shown in **Figs. 3C** and **3D,** in the 120 hrs *in vitro* corrosion tests the pH of the pure metal AZ31 soared to 8.91. The pH value was the highest among all samples during the entire corrosion process, indicating that the corrosion rate was the fastest. The pH value of the annealed AZ31 sample immobilised with F1 polypeptide coating was slightly higher than that of the AZ31 immobilised with

F3 polypeptide coating within the first 48 hrs. At 48 hrs, due to slight bacterial contamination, the pH value of the F1 immobilised sample was lower than the F3 immobilised sample, however this does not mean that the corrosion rate is slower in the later period. It was clear that the annealed AZ31 sample immobilised with F3 coating had the slowest corrosion rate and the annealed AZ31 sample immobilised with F1 polypeptide coating exhibited a corrosion rate that is considerably lower than that of bare metal annealed AZ31 sample. Both peptide coatings significantly inhibit the release of metal ions into the DMEM solution, thereby inhibiting the progress of corrosion and significantly improving the corrosion resistance of the material.

3.3.2 Weight loss

Weight loss is another indicator of corrosion. The quality analysis of the samples during the corrosion process showed that within the first 12 hrs all three samples had degraded significantly and the quality of the non-immobilised annealed AZ31 samples decreased significantly after 12 hrs (**Fig. 4**). The quality of the annealed AZ31 samples immobilised with the two peptide coatings did not change significantly within 100 hrs, especially the quality of the annealed AZ31 samples immobilised with F3 polypeptide coating. Therefore, the change of the sample mass is consistent with the change of the pH value, indicating that the material immobilised by the two polypeptides can effectively inhibit the corrosion of the material. The F3-immobilised AZ31 samples showed superior performance to both peptide F1-immobilised and no peptide-immobilised AZ31.

Fig. 4. Analysis of weight loss of different samples over 120 hrs *in vitro* corrosion tests: (A) comparison of F3 immobilised extruded AZ31 and fully annealed AZ31; (B) F1 immobilised extruded AZ31 and fully annealed AZ31; (C) three different surface conditions of annealed AZ31 samples; (D) three different surface conditions of extruded AZ31 samples.

3.4 Surface morphology and EDS analysis

After 120 hrs *in vitro* corrosion tests large cracks appeared on the surface of the annealed AZ31 sample (**Fig. 5A**), but the annealed AZ31 immobilised with the two peptides did not show any similar degradation (**Figs. 5B** and **C**). There were no significant differences of their surface morphologies before and after the *in vitro* corrosion tests, suggesting that the corrosion process of the two peptide-

immobilised materials was relatively slow and less severe. It appears that the coating prevents the contact between the Mg and the corrosion media and therefore effectively hinders the corrosion reactions of Mg samples.

Fig. 5. SEM mapping of different samples after 120-hr vitro corrosion test. (A) The surface of the metal non-immobilised with any peptides; (B) the annealed Mg alloy AZ31 immobilised with polypeptide F coating; (C) annealed AZ31 immobilised with peptide F3; (D) EDS analysis of C and MgO on the surface at 120 hrs.

Carbon and Mg oxide were analysed. The peptide contains carbon and the change in carbon was measured to determine the condition of the peptide coating. The corrosion product of Mg alloy is Mg oxide, therefore analysing the change of MgO composition can indicate corrosion of the material. After 120 hrs of *in vitro* corrosion, the annealed AZ31 sample with polyurethane (PU) coating immobilised with F3 produced the least MgO followed by the annealed AZ31 sample immobilised with F1 polypeptide coating. Annealing AZ31 produces the largest amount of MgO (**Fig. 5D**). These results indicate that bare annealing AZ31 corrodes fastest, F1 immobilised-annealed AZ31 followed by F3 peptide immobilised-annealed AZ31 samples. At the same time, the carbon content is significantly higher for peptide F1-immobilised AZ31 than F3, indicating that the F1 peptide protects against degradation more than F3.

FTIR spectra is also an effective approach to track the evolution of components and the linkage of the peptide to the coating layer. Though not employed in current research, it will be employed in future study to further demonstrate the coating of the peptide on Mg alloys.

3.5 Bacteriostatic test

The results of bacteriostatic tests were shown in **Fig. 6**. The diameter of blank disks is 7.47 mm, while the diameter of original AZ31 samples is 4.4 mm. For the purpose of analysis the results were divided into two groups for analyses according to the different sample diameters. The bacteriostatic ring was introduced to analyse the difference of the different peptide-immobilised Mg samples and positive control (Tazocin). The effective area of the bacteriostatic ring can be calculated by the following equation.

$$Ae=At-As \quad (5)$$

where, Ae is the effective area of the bacteriostatic ring and At and As are the total area and sample original area, respectively.

At and As can be obtain as

$$As=\pi r_s^2 \quad (6)$$

$$At=\pi r_t^2 \quad (7)$$

where, r_s is the original diameter of the sample and r_t is the total diameter including the effective area of bacteriostatic ring and the sample original area.

Fig. 6. Antibacterial effect analysis of different samples under different treatments: (A) Analysis of antibacterial effect of F1, F3, Tazocin and BASD; (B) Analysis of antibacterial effect of extruded AZ31, extruded AZ31+F1 and extruded AZ31+F3; (C) Analysis of antibacterial effect of annealed AZ31, annealed AZ31+F1 and annealed AZ31+F3; (D) Analysis of antibacterial effect of annealed AZ31+F1, annealed AZ31+F3, extruded AZ31+F1 and extruded AZ31+F3.

The results of the bacteriostatic tests demonstrated that: (i) Two pure metal samples (cold-drawn and annealed AZ31) have no bacteriostatic effect (**Fig. S2**); (ii) BASD do not have bacteriostatic effects (**Fig. S2**); (iii) the positive control of Tazocin has the best antibacterial effect within 24 hrs, and the antibacterial effect disappears after 24 hrs (**Fig. S2**); (iv) Both the pure peptides F1 and F3 produce a clear antibacterial effect within 24 hrs, similar to Tazocin, and the antibacterial effect disappears after 24 hrs; (v) the antibacterial effect of polypeptide F3 is significantly better than F1 polypeptide (**Fig. S2**). Both AZ31 samples immobilised with F1 peptide displayed an antibacterial effect within 24 hrs, however the antibacterial effect disappeared after 24 hrs. In contrast, F3 immobilised-annealed AZ31 samples presented excellent antibacterial behaviours within 100 hrs (**Fig. S2**). Antibacterial effect is significantly better than those of cold-drawn AZ31 samples immobilised with F1 peptide coating. Two Mg alloy AZ31 samples immobilised with F3 peptide showed a visible and lasting antibacterial effect within 100 hrs. The bacteriostatic effect showed a decreasing trend. At the same time, the antibacterial effect of the annealed AZ31 immobilised with F3 peptide is significantly better than that of the cold drawn AZ31 immobilised with F3 polypeptide coating. Since the diameter of the Mg alloy immobilised with peptide coating is very different from the diameter of Tazocin-immobilised drug-sensitive tablets there is no way to directly compare the antibacterial effect of Tazocin, hence the effective antibacterial

ring area was compared. As shown in **Figs. 4 and S2**, the annealed AZ31 sample immobilised with F3 polypeptide coating has a significantly higher bacteriostatic effect at 24 hrs than Tazocin, and the effect is also obvious after 100 hrs. In addition, the cold-drawn AZ31 metal sheet immobilised with F3 showed a lasting and significant bacteriostatic effect within 100 hrs.

4. Discussion

4.1 Advantages of the immobilisation method

Fast degradation of Mg *in vivo* significantly limits its application in medical industry. Innovations to improve the corrosion resistance of Mg has been a consistent area of interest. Many coating materials have been employed for Mg-based materials to improve their corrosion resistance. However, very few coating methods achieved ideal outcome with excellent bioactive properties adhere tightly to the Mg surface, and are environmentally friendly and biocompatible within human body [59-62].

Compared with other AMPs, caerin peptides have broad spectrum of antibacterial properties which make caerin peptides potential candidates as coating molecules. However, it is very difficult to directly apply the peptides to form a stable layer outside the Mg-based alloy. Although Mg might chelate with certain side chains (e.g., His and Lys) of caerin peptides to generate a loose layer containing peptides, this layer is likely to be deformed in physiological environment and may also lead to damage on metal surface [63]. In this study we developed a coating method using click chemistry reaction to keep metal surface intact.

Click chemistry encompasses a group of powerful, simple linking reactions. They are highly selective and specific, produce high yields, require minimal purification and are versatile in joining diverse structures without requiring protection steps [64]. Click reactions are bio-orthogonal; neither the reactants nor their products interact with functionalized biomolecules. The reactions are usually under mild or nontoxic conditions, such as at room temperature and in water [65]. As one of major classifications of click reactions, carbon-carbon multiple bonds include epoxidations, aziridinations, dihydroxylations, sulfenyl halide additions, nitrosyl halide additions, and certain Michael additions [66, 67].

Research demonstrates that most coating methods applied for Mg surface modification involve the immersion of Mg substrates in an aqueous environment [68-71]. Immersion is often fettered by the

interference of corrosion effects on the coating formation, resulting in low coating affinity/low bonding strength on the Mg surface. To avoid the effect of concomitant corrosion reaction polyurethane was chosen as a coating agent due to its lack of reactivity with Mg. This formed a stable layer that protected Mg alloy from corrosion when conducting later steps in chemical click reaction.

Surface modification of polyurethane was conducted by chemical click-response to connect with caerin peptides, which activate polyurethane through the formation of surface peroxy and hydroxyl (**Fig. 1B**). The bio-orthogonality of click reaction caused functional groups to form on the surface of polyurethane, which will assure that peptide will be chemically and firmly adhered on the polyurethane and form a complete coat of caerin peptide covering AZ31 sample' surfaces. The mixed aqueous NHS solution (pH 5.0) of 1.25 mg/ml N-hydroxysuccinimide and 5 mg/ml 1-ethyl-3- (3-dimethylaminopropyl) carbodiimide (EDC) did not show any bacterial resistance (**Fig. S1A**). This reduced interference from the environmental medium and assured that the analysis of antibacterial effect for caerin peptide would proceed much more easily and accurately.

The reaction between EDC/NHS and peptides has been reported and widely used, especially in peptide synthesis and cross-linker chemistry. Three of the pioneer studies [72, 73 and 74] can support the formation of covalent bonds. As mentioned in **Section 2.4**, the samples were ultrasonically washed twice in ultrapure water for 10 mins post peptide immobilisation, which would remove peptides largely if there were no covalent bonds involved. In addition, the comparison of antibacterial effects between samples with PU coating only (**Fig. S2**), post EDC/NHS reaction (**Fig. S1A**) and post peptide immobilisation (**Fig. 6D**) also suggested that there was peptides covalently bonding to EDC/NHS.

In addition, the procedure of coating is under optimisation to improve the bonding force by, for example, increasing contact areas between the PU coating and Mg surface, and testing PU constructed with monomers of varied polarity and functional groups. We will report the optimization in the coming study.

4.2 Effect of microstructures and membrane mechanisms on antibacterial behaviour and corrosion resistance

Caerin peptides were first isolated from Australian frogs [75-77]. Research demonstrated that caerin peptides show significant antibacterial effect on a wide spectrum of gram positive and gram-

negative bacterial strands [53]. Though many factors can contribute to the corrosion resistance of specimen, corrosion resistance of this study mainly focused on the PU immobilized peptide coating. Thickness of PU, F1 and F3 are important factors which obviously affect corrosion resistance of the coating, will be further investigated with the optimized the preparation procedure of specimen. In this study, we just investigated the possibility of employing these peptides as a coating-materials for Mg alloys.

Two properties of these peptides were investigated. Firstly, their capacity to increase the corrosion resistance of Mg alloy was assessed. Previous studies showed that certain types of PU coating can provide protection on Mg alloys from corrosion [78], yet did not present any effect of bacterial resistance. The acidic metabolites secreted/excreted by bacteria (depending on the strains) can cause further corrosion once these bacteria adhere to the surface [79]. Thus, a higher level and relatively long term of antibacterial activity possessed by the surface could also improve corrosion resistance. This was suggested in Fig. 6 that large cracks appeared on the surface of the annealed AZ31 sample without peptide immobilization, but not for the annealed AZ31 immobilised with F1 or F3; in addition, F1 and F3 immobilisation showed significantly different weight percentages of C and MgO on surface, which indicated the peptides affected corrosion resistance. Secondly, the longevity of their anti-bacterial activity, which would prevent bacterial adherence to the Mg alloy and prevent bacterial infection from unsterilised wounds, was observed. When immobilised on metal AZ31 with same condition, peptide F3 and F1 exhibited different increases in corrosion resistance and antibacterial effect, with F3 inhibiting the growth of MRSA more comprehensively than F1(**Fig. S1A**). When immersed in DMEM medium, F3 immobilised AZ31 displayed superior corrosion resistance than the peptide F1 immobilised alloy. Between 12 hrs and 48 hrs of exposure, annealed AZ31 immobilised with peptide F3 showed a lower variation of PH value than annealed AZ31 immobilised by peptide F1 (**Fig. S1B**). The change of pH value is related to variation in the concentrations of H^+ and Mg^{2+} in the medium, both of which are indicative of Mg corrosion. Minimal variation in the pH value indicates deceleration in the rate of corrosion.

Mass loss is a direct measure of the corrosion velocity. From 24 hrs to 100 hrs the mass of non-immobilised annealed AZ31 decreased much quicker than the annealed AZ31 with F1 and F3 peptide coatings. The mass of annealed AZ31 with F3 peptide coating was almost unchanged while annealed AZ31 with F1 peptide coating showed a slightly more mass loss (**Fig. 4C**). The corrosion speed of AZ31 with F3 coating is less than that of AZ31 with F1 coating (**Fig. 4C**). EDS analyses were

conducted to investigate the metal surface variation after corrosion tests. As two typical components of Mg corrosion test, C and Mg oxide were analysed (**Fig. S1C**). They were chosen because carbon is the major element of peptides and MgO is a corrosion product of Mg. Results showed that AZ31 immobilised by peptide F3 has the less C and MgO than those of AZ31 immobilised with F1. This indicates that in comparison to peptide F1 immobilised AZ31, peptide F3-immobilised AZ31 exhibited superior corrosion resistance during this *in vitro* corrosion tests.

The *in vitro* antibacterial test showed that non-immobilised annealed AZ31 did not show any bacterial resistance, while Mg alloy immobilised with F1 and F3 both showed antibacterial activity against MRSA (**Fig. 6C**). Peptide F1 immobilised annealed AZ31 exhibited an obvious antibacterial effect only within 24 hrs while annealed AZ31 with F3 coating showed considerably longer lasting bacterial resistance (up to 100 hrs). Moreover, peptide F3 immobilised AZ31 alloys with annealed or cold extruded treatment showed obviously superior bacterial resistance on MRSA compared to that of peptide F3 alone (**Fig. S1D**). Furthermore, annealed AZ31 with F3 coating showed a more pronounced and prolonged antibacterial effect compared to antibiotic Tazocin (**Fig. S1D**). Tazocin only showed bacterial resistance with 24 hrs in the current experimental setting. Though its bacterial resistance is lower than Tazocin, F1 immobilised extruded AZ31 also showed a 100 hrs antibacterial effect. All F3 immobilised samples displayed antibacterial effects over 100 hrs, while F1 immobilised AZ31 did not show these effects longer than 24 hrs.

Caerin peptides inhibit bacteria growth by membrane targeting mechanisms (MTMs) [80]. A common structural feature of AMPs is the clustering of hydrophobic and cationic residues on opposite faces of the peptide α-helix, which renders these molecules amphipathic [81-83]. The net positively charged regions bind to the negatively charged head bacterial membranes [84]. Mechanisms of action have been suggested as transmembrane pore (pore) and non-pore models [85], including the Barrel-stave model, Toroidal pore model, Carpet model and Aggregate model [86, 87] as shown in **Fig. 7**.

Fig. 7. Mechanisms of action for antibacterial HDPs and the pore forming mechanisms [80].

Peptide length is an important factor which has a significant effect on transmembrane mechanisms. If peptides are greater than 20 amino acid residues, α-helices of sufficient length can be formed to individually span a lipid membrane [88, 89]. At sufficiently high peptide concentrations, transmembrane helices may destroy the stability of bacteria membrane, or alternatively generate

barrel-stave' [90, 91] or toroidal pores [92]. These pores act as some nonselective channels through which ions, toxins and metabolites can freely flow. As a result of the preventing maintenance of homeostasis, the microbe may eventually be killed. On the other hand, peptides with less than 20 residues cannot span through a membrane individually, but are more likely to act through the "carpet" mechanism [88, 90, and 91]. This mechanism involves shorter peptides accumulating on the surface of membrane until a critical threshold forms and they solubilize or lyse the membrane like a detergent.

Besides the length, factors that determine which mechanism transpire include peptide-induced membrane thinning [93, 94] and hydrophobic mismatch [95, 96]. All mechanisms may depend on the peptide concentration relative to threshold values (e.g. alamethicin and magainin [97]). Wong et al [98] pointed out that structure and activity of caerin 1.1 interacting with membranes is similar to other antimicrobial peptides using a carpet-like mechanism. This involves individual peptides aggregating in a helical manner and orienting themselves parallel to the membrane in a sheet-like arrangement described elsewhere [99]. While Huang et al [100] found that antibacterial peptides magainin extracted from the skin of the amphibian have 23 residues and kill bacteria in a toroidal (or wormhole) model by which permeabilise the cytoplasmic membrane, they do not lyse eukaryotic cells. Peptide F1 is the modified caerin 1.1, and may have a similar antibacterial mechanism to that of caerin 1.1. Meanwhile, we observed that caerin peptide F3 has a different sequence of residues from that of F1. F3 has 25 residues while F1 have 29 residues. Though both belong to longer peptides, but they have different length of residues, thus may act as different mechanisms of killing bacteria. From the previous report, if the concentration of longer peptides exceeds the threshold value they may destabilize the bacteria membrane or span the membrane by generating a barrel-stave, toroidal pores or other models.

Interestingly, when peptide F3 was immobilised on metal AZ31, the immobilised material showed bacterial resistance for about 100 hrs, yet did not show this property when not immobilised on material (**Fig. 3B**). We suspect that a stable microstructure is formed when the peptide is immobilised on the metal surface which maintains the correct secondary microstructure of the peptides. However, it is still unclear by which mechanism peptide F3 kills bacteria. The relationship between the residues and membrane mechanism is also unknown. Therefore, further investigation is required to reach any substantive conclusion.

Conventional materials may allow the bacteria to form a bacteria biofilm which will may eventually lead to PPIs and result in a failure of an implant. F3 peptide-immobilised AZ31 has the potential to prevent bacteria (MRSA) growth when used as implanted hard tissues or internal fracture

fixing materials. This specific property may avoid the adhesion and bacterial colonization. Therefore, F peptide-immobilised AZ31 material may become an ideal implant material which exhibits both degradation decelerating and bactericidal properties.

4.3 Effect of different original treatments on corrosion resistance and coating of antibacterial peptides on Mg alloys

AZ31 with different treatment showed different behaviours in in vitro corrosion and bacteriostatic tests. The annealing or extrusion result in different surface stresses and surface microstructures, which might lead to different strengths of adhesion with PU, and consequently cause the outside of PU layer for O_2 plasma and EDC/NHS reaction differently. This could eventually impact the amount of peptide that could be covalently immobilized onto the surface. Just as showed in **Section 3.1**, coverage of F1 or F3 is obviously different between extruded AZ31 and annealed AZ31; compared to the extruded AZ31, annealed AZ31 has the less coverage of F3, but more coverage of F1. The different coverages of peptides on Mg alloys may lead to their different antibacterial abilities. Also, different corrosion resistance can lead to different lasting time of antibacterial behaviour. Thus, brief comparisons of effects of annealing and extrusion on corrosion resistance were necessary.

Fig. 8 Stress states of different samples and their coatings. (A) Stress state of cold extruded AZ31 before and after peptide coating. (B) Stress state of annealed AZ31 before and after peptide coating. (C) Schematic of H_2 pocket formation and broking process, from original coating and Mg substrate, to a formed local bulging area, to corrosion reaction in the bulging areas and forming of H_2 pocket, and final broken of H_2 pocket. SEM maps of cold extruded AZ31 immobilised by peptides F1 or F3, H_2 gas pockets appears (D) and a broken H_2 gas pocket (E).

Figs. 8A and **8B** show stress state of two samples with extruded and annealed treatment. Annealed AZ31 anneals at about 330-350°C, resulting in full recrystallization and a homogenous microstructure lacking any residual stress (**Fig. 8B**). In comparison, cold extruded AZ31 samples suffer an axial tensile force and circumferential compressive stress [101, 102] (**Fig. 8A**). In this study we did not consider the effect of hydrostatic pressure. Stresses of cold extrude AZ31 sample can be obtained by the following **Equation (8).**

$$F_E=\sigma+\tau \quad (8)$$

where, F_E is the stress state of cold extruded AZ31; σ is the axial tensile force; τ is radial compressive stress.

At the same time, coatings of the annealed or extruded AZ1 also suffer different stresses. The peptide-immobilised cold-extruded AZ31 suffer a complicated stress state F_{CE} as shown in **Fig. 8A**, which can be obtained from **Equation (9)**.

$$F_{CE}=\sigma+\tau+\alpha \quad (9)$$

where, σ is the axial thrust from the cold extruded AZ31 sample; τ is the radial shear pressure from the cold extruded AZ31 sample; α is adhesion stress between the coating and the sample.

While for the coating of annealed AZ31, the stress state is very simple and it only suffer the adhesion stress α between the coat and the sample.

The complicated stress including the shear force τ, the thrust σ and the adhere fore α may combine together to accelerate the separation of the peptide coat and the Mg substrate and further form a small bulging. This can hold a few corrosion solution (DMEM) and lead to local corrosion reaction, generating H_2 gas (**Fig. 8C**). This will form H_2 gas pockets in local areas, which can cause the separation of tissue layers [103-106]. The accumulation of H_2 gas and DMEM solution will produce a break in the surface layers with defects (e.g. cracks or thinner areas) when the stress inside the H_2 gas pocket σ_p exceeds fatigue strength (σ_f) of the local coating areas (**Fig. 8C**). Furthermore, this will produce a failure of peptide coating in these local areas [106]. This phenomenon was observed in this study. **Fig. 8D** shows some H2 gas pockets which are in the yellow colour circles. **Fig. 8E** shows a broken of H_2 gas pocket which lead to the failure of coating in these local areas.

Localised breaks in the peptide coat will obviously affect the properties (including corrosion resistance and antibacterial effect) of peptide-immobilised AZ31 sample. As shown in **Figs. 3C**, **3D** and **4**, with an increase of corrosion time the pH value of cold extruded AZ31 immobilised by F3 increased significantly within 48 hrs (7.2 to 8.47), while mass of this sample decreased (54.48 mg to 54.21 mg). Annealed AZ31 immobilised by F3 show a slightly smaller pH increase (7.2 to 8.4), while the decrease in mass was substantially smaller (58.29 mg to 58.26 mg). In the antibacterial test of MRSA the annealed AZ31 was immobilised by peptide F3 displayed a 100 hrs lasting high antibacterial effect; this effect longevity exceeds even the currently used antibiotic Tazocin, which

only showed a 24 hrs antibacterial effect (**Fig. 6**). Within 24 hrs cold extruded AZ31 immobilised by peptide F3 showed less antibacterial effect, but its antibacterial effect lasted for 100 hrs.

Conclusions

In this study, a method to immobilise host defence peptide caerin 1.9 (F3) and modified caerin 1.1 (F1) on PU immobilised AZ31 (cold extrusion and fully annealing) was developed. We found that relative to un-immobilised metal samples, the immobilisation of both peptides on PU coated AZ31 samples showed observable improvements in corrosion resistance. Moreover, F3 immobilised on AZ31 exhibited superior corrosion resistance than F1-samples. Meanwhile, both peptide-immobilised AZ31 samples displayed improved antibacterial effects, with F3 immobilisation exhibiting a longer-lasting and more notable bacterial resistance than the widely used clinical antibiotics Tazocin. The distinct antibacterial behaviours may be caused by different antibacterial mechanisms.

On the other hand, different original treatments of samples showed significant influence on corrosion resistance and antibacterial behaviours of peptide immobilised samples. Due to complicated original stress state of the cold-extruded sample, the resulted residual stresses can easily form some surface defects (like H_2 gas pockets), which can lead to a break of local coating area and accelerate the coating's failure. Conversely, more compact and uniform coating can be formed on annealed samples due to their homogeneous stresses and microstructures. All the advantages can significantly improve these samples' corrosion resistances. Also, different original treatments on samples can lead to different coverages of peptides (F1 or F3) on metal substrates, further affect their antibacterial abilities.

Another interesting observation is that excellent and long-lasting antibacterial behaviours of samples may presumably resulted from the microstructure formed by the peptide and the metal substrate. This will require further investigation.

Taken together, the current results suggested that F1 and F3 immobilised on PU-coating Mg alloys may become a promising implant material in hard tissues both inside the human body and in open wound areas.

Acknowledgements: The last corresponding author thanks Japanese JSPS committee for providing financially support of the research of Mg treatment and microstructure analysis.

Funding source: This study was supported in part by JSPS research grant (No. P16718), Foshan First People's Hospital Deng Feng project 2019A008, Foshan municipal Government (2015AG1003), Guangdong Provincial Government (2016A020213001) of China, National Natural Science Foundation of China (31971355) and Australian Research Council Discovery Project (ARC DP180103694).

Ethics declarations

The authors declare no competing interests.

References:

[1] L. Cao, L. Wang, L.Y. Fan, W.J. Xiao, B.P. Lin, Y.M. Xu, J. Liang, B.C. Cao, RGDC Peptide-Induced Biomimetic Calcium Phosphate Coating Formed on AZ31 Magnesium Alloy. Materials 10(4)(2017) 358; doi: 10.3390/ma10040358

[2] F.Witte, N. Hort, C.Vogt, S.Cohen, K.U. Kainer., R.Willumeit, F. Feyerabend, Degradable biomaterials based on magnesium corrosion. Curr. Opin. Solid State Mater. Sci. 12 (2008) 63–72.

[3] M. Navarro, A. Michiardi, O. Castano, J.A. Planell, Biomaterials in orthopaedics, J. R. Soc. Interface R. Soc. 5(2008) 1137–1158.

[4] R. Lutz, S. Srour, J. Nonhoff, T.Weisel, C.J. Damien, K.A. Schlegel, Biofunctionalization of titanium implants with a biomimetic active peptide (P-15) promotes early osseointegration, Clin. Oral Implant. Res. 21(2010) 726–734.

[5] M. Haghshenas, Mechanical characteristics of biodegradable magnesium matrix composites: A review, J. Magnes Alloy. 5(2) (2017) 189-201.

[6] A.M. Fekry, R.H. Tammam, Electrochemical Behavior of Magnesium Alloys as Biodegradable Materials in Phosphate Buffer Saline Solution, Int. J. Electrochem. Sci. 7(2012) 12254–12261.

[7] V.K. Bommala, M.G. Krishna, ChTirumala Rao. Magnesium matrix composites for biomedical applications: A review. J. Magnes Alloy. 7 (2019) 72–79.

[8] Y. Jiang, B. Wang, Z. Jia, X. Lu, L. Fang, K. Wang, F. Ren, Polydopamine mediated assembly of hydroxyapatite nanoparticles and bone morphogenetic protein-2 on magnesium alloys for enhanced corrosion resistance and bone regeneration, J. Biomed. Mater. Res. A 105 (2017) 2750–2761.

[9] A.C. Alfrey, N.L Miller, Bone magnesium pools in uremia. J. Clin. Investig. 52 (1973) 3019–3027.

[10] S. Castiglioni, A. Cazzaniga, W. Albisetti, A. Jeanette. M. Maier, Magnesium and Osteoporosis: Current State of Knowledge and Future Research Directions, Nutrients. 5(2013) 3022-3033; doi: 10.3390/nu5083022

[11] L.T. Iseri, J.H. French, Magnesium: Nature's physiologic calcium blocker, Am. Heart J. 108(1984) 188–193.

[12] F.Y. Li, B. Chaigne-Delalande, C. Kanellopoulou, J.C. Davis, H.F. Matthews, D.C. Douek, J.I. Cohen, G. Uzel, H.C. Su, M.J. Lenardo, Second messenger role for Mg2+ revealed by human T-cell immunodeficiency, Nature 475 (2011) 471–476.

[13] Li. Yang, G.W. Liu, Z.J. Zhai, L. Liu, H.W. Li, K. Yang, L.L. Tan, P. Wan, X.Q. Liu, Z.X. Ouyang, Z.F. Yu, T.T Tang, Z.N. Zhu, X.H. Qu, K.R. Dai. Antibacterial Properties of Magnesium *In Vitro* and in an *In Vivo* Model of Implant-Associated Methicillin-Resistant Staphylococcus aureus Infection, Antimicrob. Agents Chemother. 58 (12)(2014) 7586–7591

[14] A. Zomorodian, M.P. Garcia, T.M.E. Silva, J.C.S. Fernandes, M.H. Fernandes, M.F. Montemor, Corrosion resistance of a composite polymeric coating applied on biodegradable AZ31 magnesium alloy, Acta Biomater. 9 (2013) 8660–8670.

[15] H. Gao, M. Zhang, J. Zhao, L. Gao,M. Li, In vitro and in vivo degradation and mechanical properties of ZEK100 magnesium alloy coated with alginate, chitosan and mechano-growth factor, Mater. Sci. Eng. C 63 (2016) 450–461.

[16] F. Witte, V. Kaese, H. Haferkamp, E. Switzer, A. Meyer-Lindenberg, C.J. Wirth, H. Windhagen, In vivo corrosion of four magnesium alloys and the associated bone response, Biomaterials 26 (2005) 3557–3563.

[17] H.Waizy, J. Diekmann, A.Weizbauer, J. Reifenrath, I. Bartsch, V. Neubert, R. Schavan, H. Windhagen, In vivo study of a biodegradable orthopedic screw (MgYREZr-alloy) in a rabbit model for up to 12 months, J. Biomater. Appl. 28 (2014) 667–675.

[18] H. Qin, Y. Zhao, Z. An, M. Cheng, Q. Wang, T. Cheng, Q. Wang, J. Wang, Y. Jiang, X. Zhang, G. Yuan, Enhanced antibacterial properties, biocompatibility, and corrosion resistance of degradable Mg-Nd-Zn-Zr alloy, Biomaterials 53 (2015) 211–220.

[19] W. Zhang, M. Li, Q. Chen, W. Hu, W. Zhang, W. Xin, Effects of Sr and Sn on microstructure and corrosion resistance of Mg–Zr–Ca magnesiumalloy for biomedical applications, Mater. Design 39 (2012) 379–383.

[20] B. Mingo, R. Arrabal, M. Mohedano, C.L. Mendis, R. Del Olmo, E. Matykina, N. Hort, M.C. Merino, A. Pardo, Corrosion of Mg-9Al alloy with minor alloying elements (Mn, Nd, Ca, Y and Sn), Mater. Design 130 (2017) 48–58.

[21] J. Hu, H. Gao, Y.Meng, Z. Zhang, L. Gao, Effects of free-end torsion on the microstructure evolution and fatigue properties in an extruded AZ31 rod, Mater. Sci. Eng. A 726 (2018) 215–222.

[22] H.-J. Lee, J.-K. Han, S. Janakiraman, B. Ahn, M. Kawasaki, T.G. Langdon, Significance of grain refinement on microstructure and mechanical properties of an Al-3% Mg alloy processed by high-pressure torsion, J. Alloy. Compd. 686 (2016) 998–1007.

[23] C.Z. Zhang, S.J. Zhu, L.G. Wang, R.M. Guo, G.C. Yue, S.K. Guan, Microstructures and degradation mechanism in simulated body fluid of biomedical Mg–Zn–Ca alloy processed by high pressure torsion, Mater. Design 96 (2016) 54–62.

[24] C. Zhang, S. Guan, L.Wang, S. Zhu, L. Chang, The microstructure and corrosion resistance of biological Mg–Zn–Ca alloy processed by high-pressure torsion and subsequently annealing, J. Mater. Res. 32 (2017) 1061–1072.

[25] X. Wang, M. Nie, C.T. Wang, S.C. Wang, N. Gao. Micro hardness and corrosion properties of hypoeutectic Al–7Si alloy processed by high-pressure torsion, Mater. Design 83 (2015) 193–202.

[26] M. Nie, C.T. Wang, M. Qu, N. Gao, J.A. Wharton, T.G. Langdon, The corrosion behavior of commercial purity titanium processed by high-pressure torsion, J.Mater. Sci. 49 (2014) 2824–2831.

[27] W.T. Sun, X.G. Qiao, M.Y. Zheng, C. Xu, N. Gao, M.J. Starink, Microstructure and mechanical properties of a nanostructured Mg-8.2Gd-3.8Y-1.0Zn-0.4Zr supersaturated solid solution prepared by high pressure torsion, Mater. Design 135 (2017) 366–376.

[28] M. Tomozawa, S. Hiromoto, Microstructure of hydroxyapatite- and octacalcium phosphate-coatings formed on magnesium by a hydrothermal treatment at various pH values, Acta Mater. 59 (2011) 355–363.

[29] A. Zomorodian, C. Santos, M.J. Carmezim, T.M.E. Silva, J.C.S. Fernandes, M.F. Montemor, "In-vitro" corrosion behaviour of the magnesium alloy with Al and Zn (AZ31) protected with a biodegradable polycaprolactone coating loaded with hydroxyapatite and cephalexin, Electrochim. Acta 179 (2015) 431–440.

[30] F. Fan, C. Zhou, X. Wang, J. Szpunar, Layer-by-layer assembly of a self-healing anticorrosion coating on magnesium alloys, ACS Appl. Mater. Inter. 7 (2015) 27271–27278.

[31] D. Lin, F. Hung, S. Jakfar, M. Yeh, Tailored coating chemistry and interfacial properties for construction of bioactive ceramic coatings on magnesium biomaterial, Mater. Design 89 (2016) 235–244.

[32] Q. Li, W.B. Ye, H. Gao, L.L. Gao, Improving the corrosion resistance of ZEK100 magnesium alloy by combining high-pressure torsion technology with hydroxyapatite coating, Mater. Design 181 (2019) 107933.

[33] C.L. Romano, G. Manzi, N. Logoluso, D. Romano, Value of debridement and irrigation for the treatment of peri-prosthetic infections: a systematic review, Hip Int. 22 (Suppl 8) (2019):S19–S24. http://dx.doi.org/10.5301/HIP.2012.9566.

[34] R.O. Darouiche. Treatment of infections associated with surgical implants, N. Engl. J. Med. 350(2004):1422–1429. http://dx.doi.org/10.1056/NEJMra035415.

[35] A. Rava, M. Bruzzone, U. Cottino, E. Enrietti, R. Rossi, Hip Spacers in Two-Stage Revision for Periprosthetic Joint Infection: A Review of Literature, Joints 7(2) (2019): 56–63.

[36] P. Izakovicova, O. Borens, A. Trampuz, Periprosthetic joint infection: current concepts and outlook, EFORT Open Rev. 4(7) (2019): 482–494.

[37] B.P. Lazzaro, M. Zasloff, J. Rolff, Antimicrobial peptides: Application informed by evolution, Science, 368(6490) (2020) Doi: 10.1126/science.aau5480

[38] M. Kazemzadeh-Narbat, B.F. Lai, C. Ding, J.N. Kizhakkedathu, R.E. Hancock, R. Wang, Multilayered coating on titanium for controlled release of antimicrobial peptides for the prevention of implant-associated infections, Biomaterials 34(2013) 5969–5977. http://dx.doi.org/10.1016/j.biomaterials.2013.04.036.

[39] Y. Li, Y.Z. Liu, T. Long, X.B. Yu, T.T. Tang, K.R. Dai, B. Tian, Y.P. Guo, Z.A. Zhu, Mesoporous bioactive glass as a drug delivery system: fabrication, bactericidal properties and biocompatibility, J. Mater. Sci. Mater. Med. 24(2013)1951–1961. http://dx.doi.org/10.1007/s10856-013-4960-z.

[40] G. Jin, H. Qin, H. Cao, S. Qian, Y. Zhao, X. Peng, X. Zhang, X. Liu, P.K. Chu, Synergistic effects of dual Zn/Ag ion implantation in osteogenic activity and antibacterial ability of titanium, Biomaterials 35(2014) 7699–7713. http://dx.doi.org/10.1016/j.biomaterials.2014.05.074

[41] J. Lei, L.C. Sun, S.Y. Huang, C.H. Zhu, P. Li, J. He, V. Mackey, D.H. Coy, Q.Y. He, The antimicrobial peptides and their potential clinical applications, Am J Transl Res. 11(7) (2019) 3919–3931.

[42] N. Raheem, S.K. Straus. Mechanisms of Action for Antimicrobial Peptides with Antibacterial and Antibiofilm Functions, Front Microbiol. 10(2019) 2866. Published online 2019 Dec 12. doi: 10.3389/fmicb.2019.02866

[43] C. Raaymakers, E. Verbrugghe, S. Hernot, T. Hellebuyck, C. Betti, C. Peleman, M. Claeys, W. Bert, V. Caveliers, S. Ballet, A. Martel, F. Pasmans, K. Roelants, Antimicrobial peptides in frog poisons constitute a molecular toxin delivery system against predators, Nat. Commun. 8 (2017), DOI: 10.1038/s41467-017-01710-1

[44] J. Doyle, L.E. Llewellyn, C.S. Brinkworth, J.H. Bowie, K.L. Wegener, T. Rozek, P.A. Wabnitz, J.C. Wallace, M.J. Tyler, Amphibian peptides that inhibit neuronal nitric oxide synthase -The isolation of lesueurin from the skin secretion of the Australian StonyCreek FrogLitoria lesueuri, Eur. J. Biochem. 269(2002) 100-109.

[45] M.A. Apponyi, T.L. Pukala, C.S. Brinkworth, V.M. Maselli, J.H. Bowie, M.J. Tyler, G.W. Booker, J. Wallace, J.A. Carver, F. Separovic, J. Doyle, L.E. Llewellyn, Host-defence peptides of Australian anurans: structure, mechanism of action and evolutionary significance, Peptides 25 (2004) 1035–1054.

[46] M.P. Boland, F. Separovic, Membrane interactions of antimicrobial peptides from Australian tree frogs, Biochim. Biophys. Acta. 1758 (2006) 1178–1183.

[47] B.C.S. Chia, J.A. Carver, T.D. Mulhern, J.H. Bowie, Maculatin 1.1, an anti-microbial peptide from the Australian tree frog, Litoria genimaculata. Solution structure and biological activity, Eur. J. Biochem. 267 (2000) 1894–1908.

[48] T. Niidome, K. Kobayashi, H. Arakawa, T. Hatakeyama, H. Aoyagi, Structure–activity relationship of an antibacterial peptide, maculatin 1.1, from the skin glands of the tree frog, Litoria genimaculata, J. Pept. Sci. 10 (2004) 414–422.

[49] T. Rozek, R.J. Waugh, S.T. Steinborner, J.H. Bowie, M.J. Tyler, J.C. Wallace, The maculatin peptides from the skin glands of the tree frog Litoria genimaculata: a comparison of the structures and antibacterial activities of maculatin 1.1 and caerin 1.1, J. Pept. Sci. 4 (1998) 111–115.

[50] H. Wong, J.H. Bowie, J.A. Carver, The solution structure and activity of caerin 1.1, an antimicrobial peptide from the Australian green tree frog, Litoria splendida, Eur. J. Biochem. 247 (1997) 545–557.

[51] S.R. Dennison, F. Harris, D.A. Phoenix, The interactions of aurein 1.2 with cancer cell membranes, Biophys. Chemist. 127 (2007) 78–83.

[52] X. Pan, B.W. Ma, X.C. You, S. Chen, J.L. Wu, T.F. Wang, S.F. Walton, J.W. Yuan, X.L. Wu, G.Q. Chen, Y.J. Wang, G.Y. Ni, X.S. Liu, Synthesized natural peptides from amphibian skin secretions increase the efficacy of a therapeutic vaccine by recruiting more T cells to the tumour site, BMC Complement Altern Med. 19(2019) 163. Published online 2019 Jul 6. doi: 10.1186/s12906-019-2571-z

[53] B.W. Ma, J.W. Yuan, S. Chen, K.S. Huang, Q.B. Wang, J.C. Ma, R.T. Lin, L. Zhang, Y.Y. Zhou, T.F. Wang, S.F. Walton, X. Pan, G.Q Chen, Y.J Wang, G.Y Ni, X.S Liu, Topical application of temperature-sensitive caerin 1.1 and 1.9 gel inhibits TC-1 tumor growth in mice, Am J Transl Res. 12(1) (2020) 191–202.

[54] X.N. Gu, Y. Cheng, Y.F. Zheng, S.P. Zhong, T.F Xi, In vitro corrosion and biocompatibility of binary magnesium alloys, Biomaterials 30(2009): 484–98.

[55] Johnatan D, Fanny G, Claudia B, Monica M. Formation mechanisms of chitosan-silica hybrid materials and its performance as solid support for KR-12 peptide adsorption: Impact on KR-12 antimicrobial activity and proteolytic stability, jmaterrestechnol. 2020; 9(1):890–901

[56] Paints and varnishes — Cross-cut test, ISO 2409:2020(en)

[57] Standard Test Methods for Measuring Adhesion by Tape Test, ASTM D3359 - 09 E2, 2010

[58] R Nilsen, Jan Scheie, Testing the accuracy of adhesion/cohesion equipment, Protective Coatings Europe, 1996

[59] R.C. Zeng, D. Wolfgang, W. Frank, H. Norbert, B. Carsten, Progress and challenge for magnesium alloys as biomaterials, Adv Biomater. 10(8) (2008) B3–B14.

[60] S. Chen, S.K. Guan, B. Chen, W. Li, J. Wang, L.G. Wang, et al., Corrosion behavior of TiO2 films on Mg–Zn alloy in simulated body fluid, Appl Surf Sci. 257(2011) 4464–4467.

[61] H.W. Huo, Y. Li, F.H. Wang, Improvement on the corrosion resistance of AZ91D magnesium alloy by aluminum diffusion coating, J Mater Sci Technol. 23(3) (2007)379–82.

[62] J. Zhang, C.Y. Wu. Corrosion and protection of magnesium alloys – a review of the patent literature, Recent Pat Corros Sci. 2(2010)55–68.

[63] T. Wang, H.J Andreazza, T.L. Pukala, P.J. Sherman, A.N. Calabrese, J.H. Bowie, Histidine-containing host-defence skin peptides of anurans bind Cu^{2+}. An electrospray ionisation mass spectrometry and computational modelling study, Rapid Commun. Mass Spectrom. 25 (9) (2011) 1209-1221.

[64] C.D. Hein, X.M. Liu, D. Wang, Click Chemistry, a Powerful Tool for Pharmaceutical Sciences, Pharm Res. 25(10) (2008) 2216–2230. doi:10.1007/s11095-008-9616-1

[65] K. new, M.W. Brechbiel, Growing Applications of "Click Chemistry" for Bioconjugation in Contemporary Biomedical Research, Cancer Biother Radiopharm. 24(3) (2009) Doi: 10.1089=cbr.2008.0626

[66] H.C. Kolb, M.G. Finn, K.B. Sharpless, Click chemistry: diverse chemical function from a few good reactions, Angew. Chem., Int. Ed., Engl. 40(2001)2004–2021.

[67] H.C. Kolb, K.B. Sharpless, The growing impact of click chemistry on drug discovery. Drug Discov. Today. 8(2003) 1128–1137.

[68] G.Y. Liu, J. Hu, Z.K. Ding, C. Wang, Bioactive calcium phosphate coating formed on micro-arc oxidized magnesium by chemical deposition, Appl Surf Sci. 257(2011) 2051–2057.

[69] S. Shadanbaz, G.J. Dias, Calcium phosphate coatings on magnesium alloys for biomedical applications: a review, Acta Biomater. 8(2012) 20–30.

[70] S. Keim, J.G. Brunner, B. Fabry, S. Virtanen, Control of magnesium corrosion and biocompatibility with biomimetic coatings, J Biomed Mater Res B Appl Biomater. 96B (1) (2011) 84–90.

[71] H. Hornberger, S. Virtanen, A.R. Boccaccini, Biomedical coatings on magnesium alloys – a review, Acta Biomater. 8(2012) 2442–2455.

[72] Anderson, G.W.; Zimmerman, J. F.; Callahan, F. M. (1963). "N-Hydroxysuccinimide Esters in Peptide Synthesis". J. Am. Chem. Soc. 85 (19): 3039. doi:10.1021/ja00902a047.

[73] Grabarek, Z. and Gergely, J. (1990). Zero-length crosslinking procedure with the use of active esters. Anal Biochem 185:131-5. Staros, J.V., et al. (1986).

[74] Enhancement by N-hydroxysulfosuccinimide of water-soluble carbodiimide-mediated coupling reactions. Anal Biochem 156:220-2.

[75] S.T. Steinborner, R.J. Waugh, J.H. Bowie, J.C. Wallace, M.J. Tyler, S.L. Ramsay, New caerin antibacterial peptides from the skin glands of the Australian tree frog Litoria xanthomera, J Pept Sci. 3(3) (1997):181-185.

[76] S.T. Steinborner, R.J. Waugh, J.H. Bowie, M.J. Tyler, New Caerin Antibacterial Peptides from the Skin Glands of the Australian Tree Frog Litoria xanthomera. Part 2. Sequence Determination Using Mass Spectrometry and Associated Techniques, Rapid Commun. Mass Spectrom. 11(1997) 997-1000.

[77] S.T. Stejnborner, G.J. Currie, J.H. Bowie, J.C. Wallace, M.J. Tyler, New antibiotic caerin 1 peptides from the skin secretion of the Australian tree frog Litoria chloris. Comparison of the activities of the caerin 1 peptides from the genus Litoria, J. Peptide Res. 51(1998) 121-126.

[78] J. Zhang, H. Huang, J. Ma, L. Huang, L. Huang, X. Chen, H. Zeng, S. Ma. Preparation and Properties of Corrosion-Resistant Coatings From Waterborne Polyurethane Modified Epoxy Emulsion, Front. Mater, (6)2019, doi:10.3389/fmats.2019.00185

[79] Kip, J.Veen. The dual role of microbes in corrosion, The ISME Journal (2015) 9, 542–551.

[80] N. Raheem, S.K. Straus, Mechanisms of Action for Antimicrobial Peptides with Antibacterial and Antibiofilm Functions, Front. Microbiol. 10 (2019) 2866, doi: 10.3389/fmicb.2019.02866

[81] S.E. VanCompernolle, R.J. Taylor, K. Oswald-Richter, J.Y. Jiang, B.E. Youree, J.H. Bowie, et al., Antimicrobial Peptides from Amphibian Skin Potently Inhibit Human Immunodeficiency Virus Infection and Transfer of Virus from Dendritic Cells to T Cells, J. Virol, 79(18) (2005) 11598–11606 doi:10.1128/JVI.79.18.11598–11606.2005

[82] P. Nicolas, A. Mor, Peptides as weapons against microorganisms in the chemical defense system of vertebrates. Annu. Rev. Microbiol. 49(1995) 277–304.

[83] A.C. Rinaldi, Antimicrobial peptides from amphibian skin: an expanding scenario, Curr. Opin. Chem. Biol. 6(2002) 799–804.

[84] K. Matsuzaki, Why and how are peptide-lipid interactions utilized for self-defense? Magainins and tachyplesins as archetypes, Biochim. Biophys. Acta 1462(1999)1–10.

[85] P. Kumar, J. N. Kizhakkedathu, S.K. Straus, Antimicrobial Peptides: Diversity, Mechanism of Action and Strategies to Improve the Activity and Biocompatibility In Vivo, Biomolecules 2018, 8(4) (2018) doi:10.3390/biom8010004

[86] D.I. Fernandez, J.D. Gehman, F. Separovic, Membrane interactions of antimicrobial peptides from Australian frogs, Biochimica et Biophysica Acta. 1788 (2009) 1630–1638

[87] Z. Oren, Y. Shai, Mode of action of linear amphipathic α-helical antimicrobial peptides, Biopolymers (Peptide Science) 47 (1999) 451–463.

[88] Y. Shai, Mechanism of the binding, insertion and destabilisation of phospholipid bilayer membranes by α-helical antimicrobial and cell non-selective membranelytic peptides, Biochim. Biophys. Acta 1462 (1999) 55–70.

[89] Y. Shai, Z. Oren, From "carpet" mechanism to de-novo designed diastereomeric cell-selective antimicrobial peptides, Peptides 22 (2001) 1629–1641.

[90] L. Yang, T.A. Harroun, T.M. Weiss, L. Ding, H.W. Huang, Barrel-stave model or toroidal model? A case study on melittin pores, Biophys. J. 81 (2001) 1475–1785.

[91] F.Y. Chen, M.T. Lee, H.W. Huang, Evidence for membrane thinning effect as the mechanism for peptide-induced pore formation, Biophys. J. 84 (2003) 3751–3758.

[92] M.T. Lee, W.C. Hung, F.Y. Chen, H.W. Huang, Mechanism and kinetics of pore formation in membranes bywater-soluble amphipathic peptides, Proc. Natl. Acad. Sci. U. S. A. 105 (2008) 5087–5092.

[93] M.R.R. de Planque, B.B. Bonev, J.A.A. Demmers, D.V. Greathouse, R.E. Koeppe II, F. Separovic, A. Watts, J.A. Killian, Interfacial anchor properties of tryptophan residues in transmembrane peptides can dominate over hydrophobic matching effects in peptide–lipid interactions, Biochemistry 42 (2003) 5341–5348.

[94] S. Ozdirekcan, T.K.M. Nyholm, M. Raja, D.T.S. Rijkers, R.M.J. Liskamp, J.A. Killian, Influence of trifluoroethanol on membrane interfacial anchoring interactions of transmembrane α-helical peptides, Biophysical Journal 94 (2008) 1315–1325.

[95] B. Bechinger, Structure and function of membrane-lytic peptides, Crit. Rev. Plant Sci. 23 (2004) 271–292.

[96] S.J. Ludtke, K. He, W.T. Heller, T. A. Harroun, L. Yang, H.W. Huang, Membrane Pores Induced by Magainin, Biochemistry 35(1996) 13723-13728.

[97] Y. Shai, Molecular recognition between membrane-spanning polypeptides, Trends Biochem. Sci. 20(1995) 460-464.

[98] H. Wong, J. H. Bowie, J.A. Carver. The solution structure and activity of caerin 1.1, an antimicrobial peptide from the Australian green tree frog, Litoria spzendida, Eur. J. Biochem. 247(1997) 545-557.

[99] J. Yuan, X. You, G. Ni, T. Wang, S. Cavezza, X. Pan, X. Liu, Iodine-125 labeled Australian frog tree host-defense peptides caerin 1.1 and 1.9 better inhibit human breast cancer cells growth than the unlabeled peptides. (125)I-caerin 1.9 may better be used for the treatment of breast cancer, Hell J Nucl Med. 21(2018) 115-120.

[100] K. Sofinowski, T. Panzner, M. Kubenova, J. Capek, S. Van Petegem, H. Van Swygenhoven, In situ tension-tension strain path changes of cold-rolled Mg AZ31B, Acta Mater.. 164 (2019) 135-152.

[101] J.M. Atienza, M.L. Martinez-Perez, J. Ruiz-Hervias, F. Mompean, M. Garcia-Hernandez, M. Elices. Residual stresses in cold drawn ferritic rods, Scr. Mater. 52 (2005) 305–309.

[102] W. Cui, E. Beniash, E. Gawalt, Z. Xu, C. Sfei. Biomimetic coating of magnesium alloy for enhanced corrosion resistance and calcium phosphate deposition. Acta Biomater. 9(2013) 8650–8659.

[103] X. Gu, Y. Cheng, Y. Zheng. S. Zhong Shengping, T Xi, In vitro corrosion and biocompatibility of binary magnesium alloys, Biomaterials 30(2009) 484–498.

[104] G. Song, Control of biodegradation of biocompatible magnesium alloys, Corr Sci. 2007;49(2007)1696–1701.

[105] A. Meyer-Lindenberg, H. Windhugen, F. Witte, US200410241036

[106] N.T. Kirkland, N. Birbilis, M.P. Staiger, Assessing the corrosion of biodegradable magnesium implants: a critical review of current methodologies and there limitations, Acta Biomater. 8(2012) 925–936.

Figures

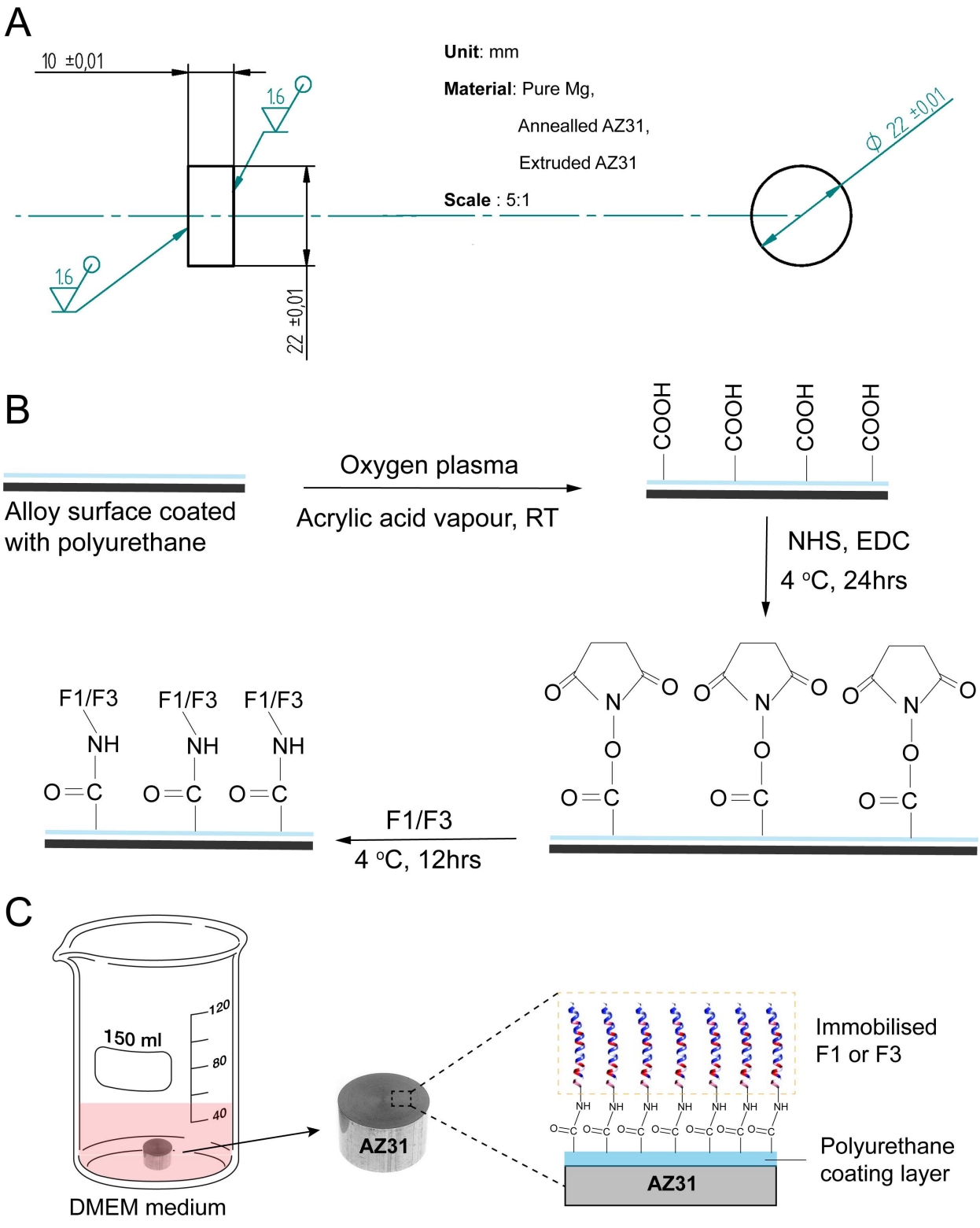


Figure 1

Mg alloy fabrication and peptide immobilisation procedure. (A) Schematic of Mg samples and all size parameters; (B) Surface modification of polyurethane coating Mg alloy by chemical click-reaction using O2 plasma; (C) Mg alloy immobilised by polyurethane and immobilisation of F1 or F3 on surface.



Figure 2

Surfaces of different specimens: (A) Mg alloy only; (B) Mg alloy with PU coating, and (C) PU coated Mg alloy after bonding force test.

Figure 3

Microstructure of annealed AZ31 (A) and cold extrude AZ31 (B). Analysis of pH of different samples during in vitro corrosion test: (C) Extruded AZ31, extruded AZ31 immobilised by F1, and extruded AZ31 immobilised by F3. (D) Annealed AZ31, annealed AZ31 immobilised by F1, and annealed AZ31 immobilised by F3.

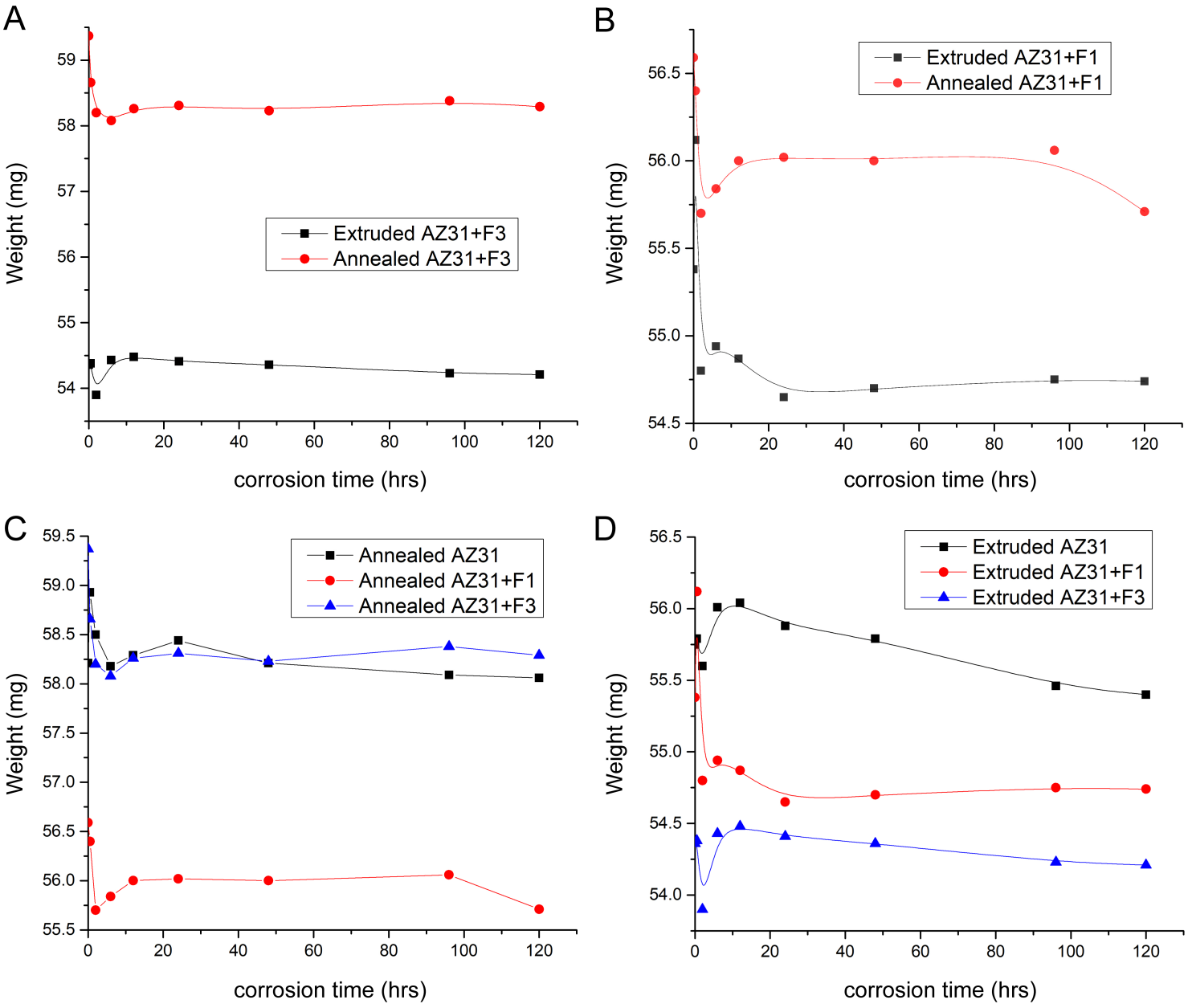


Figure 4

Analysis of weight loss of different samples over 120 hrs in vitro corrosion tests: (A) comparison of F3 immobilised extruded AZ31 and fully annealed AZ31; (B) F1 immobilised extruded AZ31 and fully annealed AZ31; (C) three different surface conditions of annealed AZ31 samples; (D) three different surface conditions of extruded AZ31 samples.

Figure 5

SEM mapping of different samples after 120-hr vitro corrosion test. (A) The surface of the metal non-immobilised with any peptides; (B) the annealed Mg alloy AZ31 immobilised with polypeptide F coating; (C) annealed AZ31 immobilised with peptide F3; (D) EDS analysis of C and MgO on the surface at 120 hrs.

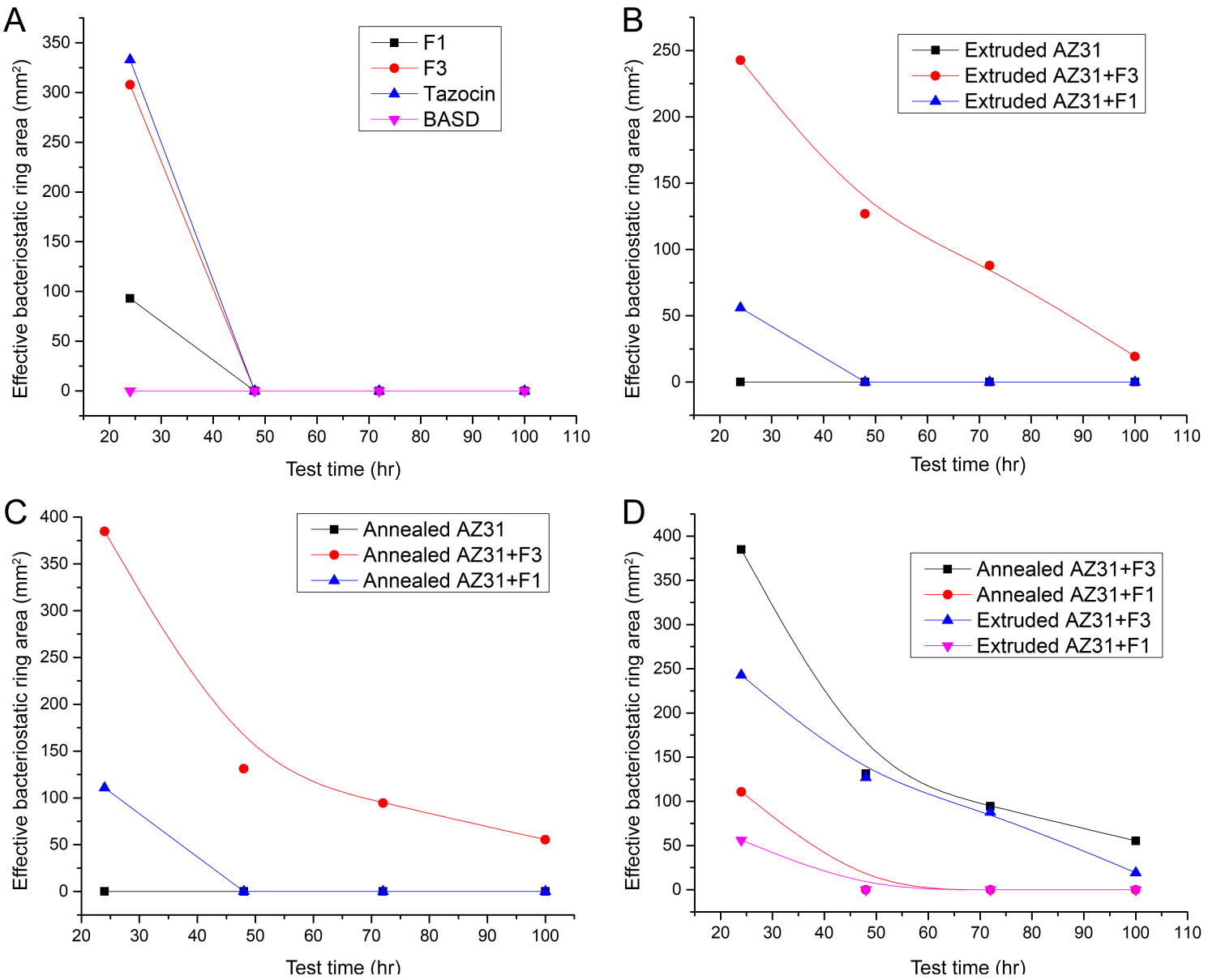


Figure 6

Antibacterial effect analysis of different samples under different treatments: (A) Analysis of antibacterial effect of F1, F3, Tazocin and BASD; (B) Analysis of antibacterial effect of extruded AZ31, extruded AZ31+F1 and extruded AZ31+F3; (C) Analysis of antibacterial effect of annealed AZ31, annealed AZ31+F1 and annealed AZ31+F3; (D) Analysis of antibacterial effect of annealed AZ31+F1, annealed AZ31+F3, extruded AZ31+F1 and extruded AZ31+F3.



Figure 7

Mechanisms of action for antibacterial HDPs and the pore forming mechanisms [80].

Figure 8

Stress states of different samples and their coatings. (A) Stress state of cold extruded AZ31 before and after peptide coating. (B) Stress state of annealed AZ31 before and after peptide coating. (C) Schematic of H2 pocket formation and broking process, from original coating and Mg substrate, to a formed local bulging area, to corrosion reaction in the bulging areas and forming of H2 pocket, and final broken of H2 pocket. SEM maps of cold extruded AZ31 immobilised by peptides F1 or F3, H2 gas pockets appears (D) and a broken H2 gas pocket (E).

Supplementary Files

This is a list of supplementary files associated with this preprint. Click to download.

- TableS1.xlsx
- TableS2.xlsx
- FigureS1.tif
- FigureS2.docx